JOURNAL OF MATERIALS SCIENCE 31 (1996) 1767–1778

Electrodeposition of Ni and Co in low gravity

H. ABI-AKAR, C. RILEY
Department of Chemistry and Materials Science, The University of Alabama in Huntsville, Huntsville, AL, 35899, USA

G. MAYBEE
McDonnell Douglas Aerospace Company, Huntsville, AL, 35814, USA

Electrodeposition of Ni and Co metals under low gravity conditions was investigated, with emphasis on Ni. Custom designed experimental packages aboard sounding rockets were utilized for this purpose. Four missions were employed each providing 7 min of electrodeposition at $\sim 10^{-4}$ g. Several deposition conditions were studied including current density, electrolyte composition, substrate nature and deposition cell configuration. High current deposition, encompassing or exceeding 80 mA cm^{-2} produced Ni films in the nanocrystalline size range in a reduced gravity environment. Under the same conditions, Earth-produced deposits were crystalline and discontinuous. The convectionless deposition, achieved in low gravity, produced structural anomalies in Ni under specific conditions. Process efficiency and corrosion behaviour for the surfaces were also different in the two environments. The low gravity environment did not affect the electrochemical factors influencing Co deposition for the limited conditions we were able to study. No structural differences were observed between Co deposits in the two environments.

1. Introduction

An accelerated paced research in materials development and characterization has been observed in the past ten years [1]. This movement has been motivated by the demands for new materials with a variety of complicated applications. Amorphous metals and metallic alloys have occupied a major area of this research; metallic amorphous alloys are widely used in various industrial applications due to their outstanding mechanical, magnetic, electrical, corrosion and catalytic properties [2]. Further demand for materials with properties beyond the present limitations has stimulated research into generating new forms of materials. As a result, the new field of nano-crystalline materials has blossomed. These materials are characterized by single or multiphase polycrystals, with sizes of the order of 1–100 nm. Their atomic arrangement allows unique properties and applications such as easy to fabricate ceramics which are stronger and tougher than conventional products, significantly harder metals, magnetic and transparent polymers, and combinations of magnetic, electrical and optical properties that are not available in conventional materials [3].

The preparation methods employed for amorphous or nanocrystalline forms generally involve rapid cooling techniques such as melt quenching, gas-phase condensation, sputtering, ion implantation, and electro or electroless deposition. Electroless deposition has been used extensively to produce the well known and widely used amorphous Ni–P alloys [4]. The availability of a low gravity environment for research has opened a new frontier for materials research. However, due to cost, inconvenience to the general interactive experimental regimen and inability to gain continual access to flights, experimentation has been sparse. Initially, experimentation that took place focused on crystallization of proteins or detector-type materials [5, 6]. Crystallization is influenced significantly by convection, and these light weight valuable substances were excellent candidates to prove the utility and justification of expensive low gravity experimentation. Other types of low gravity materials experiments have become more common place especially as accessibility and simplification of safety requirements have been reduced by new carrier vehicles or modes such as sounding rockets or shuttle GAS cans [7]. Low gravity electrodeposition falls into this latter category of experimentation.

We recently published results on the electrodeposition of neat Ni in the low gravity environment produced during KC-135 aircraft parabolas [8]. This simple and cheaper low gravity experiment attempted to reproduce the exciting results of Ehrhardt [9–12] who carried out a series of Ni electrodeposition experiments on sounding rockets. Whereas his experiments led to nondiffracting Ni deposits, ours only resulted in highly crystalline face centred cubic nickel. Thus we were left with the dilemma on why the KC-135 experiments did not reproduce similar experiments performed on a sounding rocket. Several reasons for the apparent disparity include difference in the gravity level $\sim 10^{-2}$ g versus $\sim 10^{-4}$ g (1 g = earth), and the shorter duration of the KC-135 low gravity, about

0022–2461

20–25 s versus 6–7 min on a sounding rocket. Also the multiple accumulations of 20 s length (KC-135) are interspersed with 2–3 g segments which remix the electrodeposition cells' solutions and/or suspensions while they are not operational.

These seemingly conflicting results indicated a need to undertake a comprehensive approach for studying the low gravity (LG) effects on electrodeposition of nickel and an additional metal, Co, under various preset conditions. Co electrodeposition was chosen because of its similar electrodeposition characteristics and important metallic properties [13]. The parameters varied in our low gravity electrodeposition experiments encompassed current, electrolytic solution, substrate and electric mode (galvanostatic or potentiostatic). Characterization of the deposits focused on structural and electrochemical aspects, as well as corrosion behaviour of the LG obtained samples. The conveyance vehicles utilized for our LG electrodeposition studies were commercial sounding rockets.

2. Experimental procedure

2.1. Electrodeposition process

Ni and Co were electrodeposited under gravity conditions of the order of 10^{-4}–10^{-6} g for about 7 min on three sounding rockets (Consorts I, III and IV). Multicell electrodepositions were performed on each flight in specially designed plexiglass cells (Fig. 1). A variation of this cell, where the cathode was mounted on a pedestal extending inside the cell cavity, was used in Consort IV and designated Close-Electrode cell (CE). The cathode–anode separation was 0.5 cm in the CE cell, versus 3.5 cm in the regular cell. The cells were sealed free of gas bubbles after filling with electrolytic solutions that included:

Ni	Solution Ia	Nickel sulfamate	$(H_2NSO_3)Ni \cdot 4H_2O$	600 g l^{-1}
		Nickel chloride	$NiCl_2 \cdot 6H_2O$	25 g l^{-1}
		Boric acid	H_3BO_4	30 g l^{-1}
		pH 3.5–4.0		
	Solution Ib	Nickel sulfate	$NiSO_4 \cdot 6H_2O$	375 g l^{-1}
		Nickel chloride	$NiCl_2 \cdot 6H_2O$	45 g l^{-1}
		Boric acid	H_3BO_4	37 g l^{-1}
		pH 2.5–3.0		
Co	Solution II	Cobalt sulfate	$CoSO_4 \cdot 7H_2O$	500 g l^{-1}
		Sodium chloride	NaCl	17 g l^{-1}
		Boric acid	H_3BO_4	20–35 g l^{-1}
		pH 4.0–5.0		

All electrolytic solutions were 0.2 μm filtered, deoxygenated by a N_2 purge for 20 min and degassed under vacuum before use.

Substrate materials were chosen to be inert to eliminate any reaction with the solution during the period that follows experiment assembly and precedes the flight (36 h for rocket flights). Gold electroplated Cu plates or glassy carbon (GC) were the materials of choice. In the former, the 1 sq. in. Cu plate was polished to a 0.5 μm finish before depositing at least 5 μm of gold. For the close-electrode cell, 1 cm^2 Cu discs were similarly prepared. GC plates were purchased with a mirror finish and required minor buffing only. The nature of the substrates as well as their treatment discouraged epitaxial deposit growth. Anodes, either pure Ni or Co, were pickled in suitable acid mixtures and ultrasonically cleaned in high resistivity DI water. Low gravity electrodeposition cells were run either potentiostatically or galvanostatically. Electronic boards or dedicated computers controlled the inputs and recorded the outputs of the electrodeposition processes. In the original version of our apparatus, cells and supporting electronics were simply mounted on 0.25 inch thick aluminium base plates which were in turn bolted to longeron supports provided for the experiment integration. In a later version the cells were mounted in an enclosed detachable box which not only served as another level of confinement for possible shuttle experimentation but enabled us to prepare totally off site for rocket launches. An example of our latest computer controlled package is

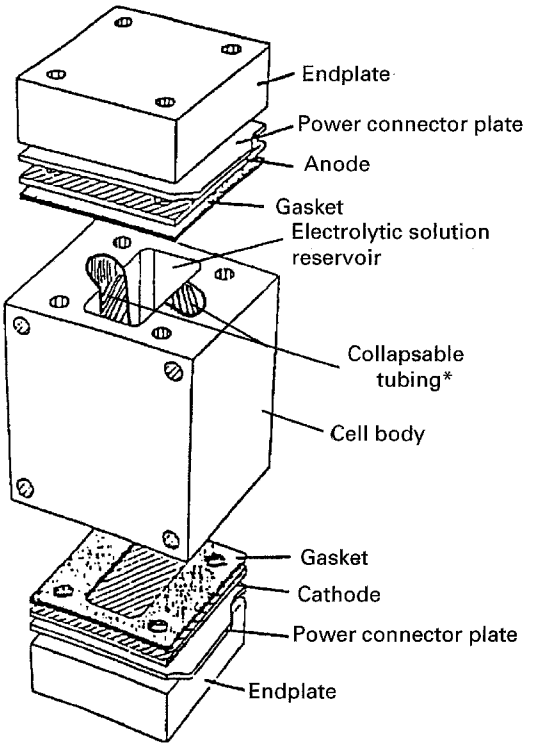

Figure 1 Electrodeposition cell, where * indicates pressure compensating feature.

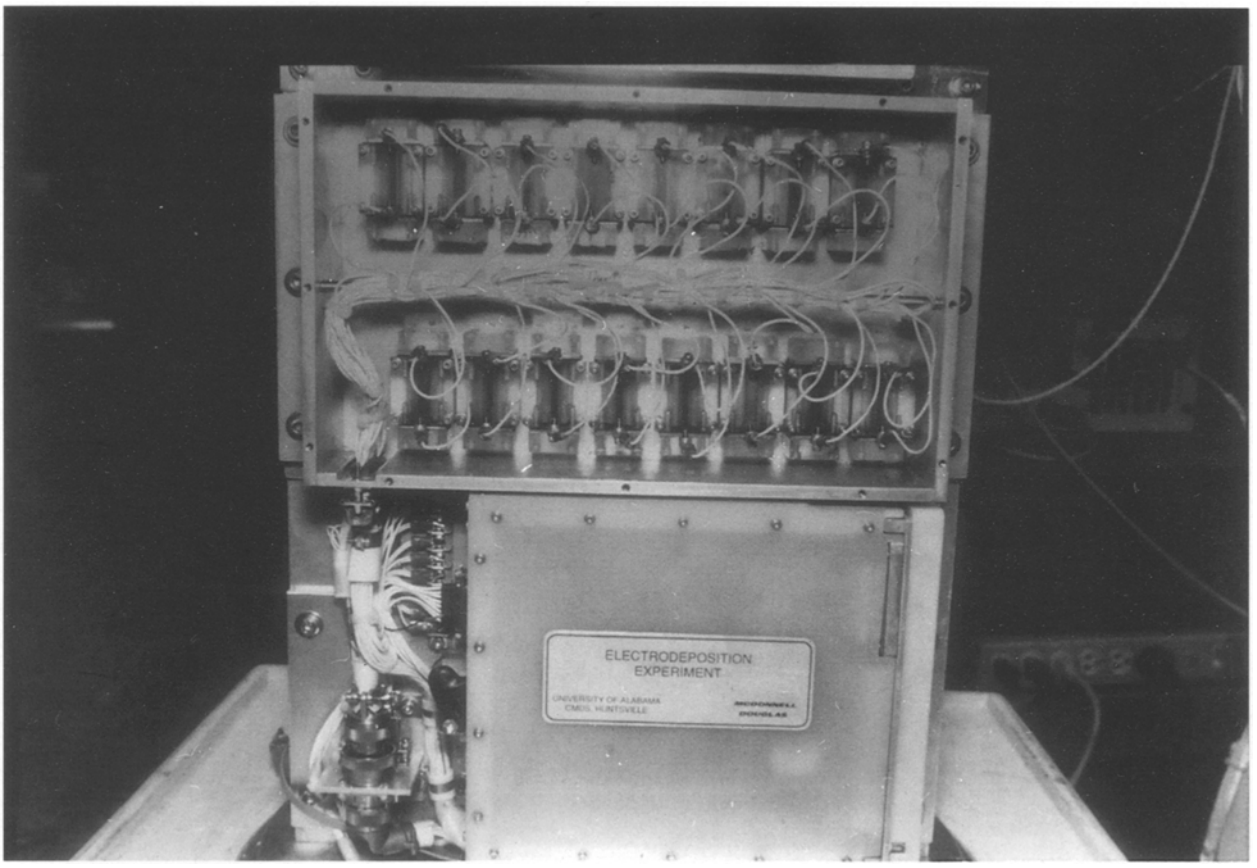

Figure 2 Consort IV experimental plate. The aluminium/teflon box houses a 12 bit memory Tattletale computer and interface electronic boards.

shown in Fig. 2. Each experiment had to pass safety requirements that included vibration, spin, leakage and freeze tests. There were size, weight and power restrictions as well as gravity noise restrictions imposed. Safety documentation was required for each rocket flight, and although more extensive than for KC-135 experimentation, it was still minor relative to that required for shuttle flights.

1 g reference cells were prepared similarly and run on the bench using the same experimental hardware. To simulate the diffusion driven LG electrodeposition process, the cells were operated in a vertical configuration placing the flat electrodes perpendicular to the gravity vector, with the cathode above the anode. This allowed the dense solution generated by the oxidation half reaction to be trapped at the bottom of the cell, while the light solution layer depleted by the reduction half reaction was trapped by the cathode. The arrangement promotes diffusion controlled mass transfer. Even with this arrangement on the bench, some convection would be expected since, at high operating current, gases generated during the process would travel to the top of the cell producing a stirring action. In a LG environment, gas bubbles would remain stationary at the source of their generation.

The electrodeposition processes in the first flight were dedicated to a current/rate study on the Ni system employing Au cathodes and a Ia electrolytic solution. One of the routes followed to study the effects of increasing current was to successively increase the voltage by 1.5 V increments on four cells from 4.5 to 9 V. These applied potentials allowed for an increasing current that would progress to the value produced in the earlier TEXUS programme studies [9–12]. Subsequent flights were dedicated to high current Ni deposition under varying parameters such as bath composition and substrate nature, and current rate Co deposition from a II solution at 4 and 5 V. Current/voltage inputs and outputs were sampled every second throughout the electrodeposition. Their chronographs aided in identifying differences between LG and 1 g processes and dominating electrochemical factors. Temperature was not controlled but was recorded at one second intervals with the aid of a thermistor.

2.2. Sample characterization

Surface morphology of the deposits was observed using scanning electron microscopy (SEM). Transmission electron microscopy (TEM) was utilized to study the microstructure and to obtain electron diffraction patterns (DP) of some Ni deposits. The crystallinity of the deposits was accessed by an X-ray diffractometer (XRD), fitted with a Cu target and graphite monochromator. Samples which showed broadened low-intensity diffraction peaks were further analysed using Sherrer and Fourier methods. For this purpose, slow scans, $1^\circ\ min^{-1}$, of the Ni(2 0 0) diffraction peak (which does not overlap with any Au substrate diffraction peaks), were studied. Following a Fourier approach, sample peaks were deconvoluted to separate

instrumental and crystal size broadening effects. The standard utilized was a sintered Ni sample assumed to approximate infinite size crystals. In order to apply the Fourier and Sherrer methods, the slow scans were transformed into data tables of intensity versus diffraction angle via an "Un-Plot-It" software facility (Silk Scientific). The same software provided peak area values utilized in the Sherrer equation. Data tables of the various samples were managed through the utilization of spread sheet programs to fall into the same diffraction angle interval and possess the same number of data points as required for Fourier analysis. The analysis was performed utilizing "Mathcad" software [13]. This approach resulted in an estimate of average crystal sizes and size distribution in the low gravity deposits.

Deposit thickness of the different samples was determined by: (1) depositing Cu on the samples, cross-sectioning, mounting in an epoxy resin, polishing, and observing by optical microscopy, or (2) profilometry and gravimetric means. Cathodic current efficiency of each deposition process was determined by comparing the measured thickness of the samples to that predicted by Faraday's law for 100% current efficiency.

LG deposits were corrosion tested and compared to their 1 g similarly prepared counterparts, as well as to that of commercially obtained sheets. Two different methods were followed depending upon the physical nature of the samples. The cross-sectioned samples were tested by exposure to a corrosive medium. The Cu surrounding the Ni film was selectively dissolved in an aqueous solution of 50 $g l^{-1}$ sulfuric acid and 500 $g l^{-1}$ chromic acid, and the surfaces then swabbed with a fresh solution of 50% nitric acid + 50% acetic acid for 30 s. This acid mixture attacks grain boundaries preferentially [14]. The extent of the attack was inspected by optical microscopy. Cyclic voltammetry (CV) was used to test the remaining LG samples (Consorts III, and IV) and 1 g counterparts. The test medium was sea water, deoxygenated by an N_2 purge before each sample exchange.

3. Results and discussion

3.1. Nickel

Table I summarizes the Ni deposition parameters utilized in the three flights as well as some of the results obtained.

3.1.1. Electrochemical aspects

A current/rate study of Ni deposition on Consort I showed that utilizing a voltage progression in our identical cells from 4.5 to 9 V resulted in low gravity cell current densities between 35 and 80 mA cm^{-2}. Apparent differences are noted between LG and 1 g current profiles (Fig. 3a and b), reflecting variant controlling factors in the two environments. Convection cannot be completely suppressed in 1 g due to gas hydrodynamics, while diffusion controlled transport is expected under LG conditions.

LG galvanostatic control at 80 mA cm^{-2} or higher produced Ni deposits that exhibited cracking, nonuniformity, and in some cells no deposition. Assuming Nernstian kinetics, i.e. fast irreversible kinetics with a diffusion limited system, the Sand equation [15, 16] describes the galvanostatic LG electrodeposition of Ni:

$$C(x,t) = \bar{C} + \frac{i\nu}{nF}\frac{1}{\pi^{1/2}D^{1/2}}\int_0^t \frac{1}{t^{1/2}}\exp\left(\frac{-x}{4Dt}\right)dt \quad (1)$$

where C is the molar concentration (mol l^{-1}), $\bar{C}$ is the molar bulk concentration (mol l^{-1}), i is the current density (A cm^{-2}), F is Faraday's constant (96487 C equiv^{-1}), n is the number of electrons involved in the electrode reaction, D is the diffusion coefficient (cm^2 s^{-1}), t is the time (s), x is the distance from the electrode, and ν is the number of cations into which a molecule dissociates.

The time required for the concentration of the active species to reach zero at the surface is called the transition time, τ (s). Determined from the Sand

TABLE I Low gravity Ni electrodeposition parameters and outputs

	Sample	Bath	Substrate	Input (V)	Output[a] (mA cm^{-2})	Efficiency (%)
Con I	1	Ia	Au	4.5	35	100
	2	Ia	Au	6.0	54.0	77
	3	Ia	Au	7.5	72.0	35
	4	Ia	Au	9	83.0	10
Con III	1 stirred	Ia	Au	8.0	83.0	54
	2	Ia	Au	9.0	78.0	16
	3	Ib	Au	9.0	77.0	16
	4	Ia	GC	9.0	86.0	79
Con IV	1	Ia	Au	9.0	70.0	–
	2	Ib	Au	9.0	60.0	–
	3	Ib	Au	4.8	75.0	–
	CE** cell					

[a] Average values.
[b] Fig. 1b, Solution Ia: sulfamate, Ib: sulfate.

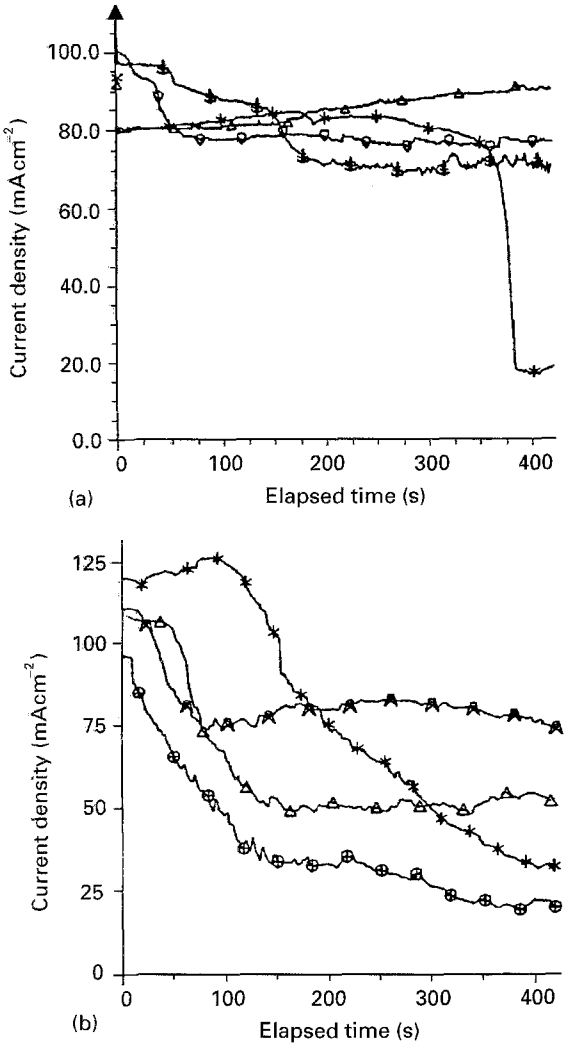

Figure 3 Current profiles of potentiostatic Ni electrodeposition for (a) LG (Consort III) and (b) its 1 g counterpart. (a) Key: * LG, sulfamate (stirred), 8.5 V, Au; LG, sulfamate, 9 V, Au; ▽ LG, sulfate, 9 V, Au; △ LG, sulfamate, 9 V, GC. (b) Key: * 1 g, sulfamate, 9 V, GC; ⊕ 1 g, sulfate, 9 V, Au; △ 1 g, sulfamate, 9 V, Au; A 1 g, sulfamate (stirred), 9 V, Au.

equation, τ, can be expressed as:

$$\tau = \frac{\pi}{4} D \left(\frac{nF}{iv} \bar{C} \right)^2 \quad (2)$$

τ is inversely proportional to the square of the current, implying faster decrease of the deposited species concentration at the surface with increasing input current. The relationship between the transition time and the overvoltage η (V), assuming equilibrium conditions and using the Nernst equation, is:

$$\eta = \frac{RT}{nF} \sum \nu \ln[1 \pm (t/\tau)^{1/2}] \quad (3)$$

Hence, theoretically, at the cathode (− ve sign by convention) as t approaches τ, diffusion overpotential tends to infinity. This implies that a process other than Ni deposition, such as gas generation dominates. Using our flight system condition, application of Equation 2 yields a τ value of 86.00 s. During this transition time, Ni deposition and hydrogen evolution are taking place due to the high current and low overpotential of hydrogen on Au. The evolving gas would have a profound effect in the closed cell in LG, where it is trapped at the cathode. Hydrogen would introduce stresses to the plated Ni, it can act as a cleaning process, removing some of the deposit, and eventually masking the cathode completely and shutting the process off. These factors may explain the low efficiency of the process, poor quality of the deposit, and lack of deposition in some cells. Under the same conditions, deposition on GC promoted higher efficiency than on Au. This result is attributed to the higher hydrogen overvoltage on the former, as well as to the amorphous character of GC. Amorphous materials have been found to be very effective catalysts, hence the GC substrate may catalyse the deposition process.

Potentiostatically-controlled LG deposition produced uniform plating on Au and GC from solutions Ia and Ib. Current chronographs of the LG and 1 g experiments (Fig. 3) exhibited remarkable differences. While the current decreased with time in a 1 g plating process, it remained steady under LG conditions. This behaviour was attributed to different controlling factors in the two environments, implying that mass transport plays an important role in the Ni plating system. Deposit quality in LG was superior to that of 1 g. Lack of gravitational force resulted in uniform continuous deposits, while, nonuniform, discontinuous and thin deposits were obtained in Earth-based experiments.

3.1.2. Morphological aspects

SEM and TEM micrographs revealed that deposit morphology was strongly dependent on the deposition current and substrate. Grain size decreased as the current increased, confirming the effects of current density on the texture, crystal size and uniformity [14, 17–20]. On Consort I, as the current was increased the surface features of the Ni deposits changed markedly (Fig. 4a to d). The nickel deposited on Au at 9 V show no recognizable surface features other than gas pocks at 3000 magnification. In subsequent flights similar behaviour was noticeable, although some crazing was associated with certain deposits. Differences between 1 g and LG deposit morphologies produced on Consort IV are very apparent in Fig. 5a and b for Ni on Au at 5000 magnification. Earth-based samples exhibited nodular Ni growth of up to 5 μm diameter, while the LG counterparts had very fine surface formations. SEM secondary electron emission of galvanostatically controlled Au prepared surfaces did not reveal any deposits, but high magnification backscattered electrons showed the occurrence of nucleation of Ni on Au. These nuclei emulated three-dimensional crystallites (TDC). Weil and Wu [21] have proposed TDCs to mark the initiation of non-epitaxial growth which result in fine grained samples. The growth of these crystallites was apparently hindered by severe conditions such as gas evolution and/or very high overpotentials in agreement with the explanation proposed in conjunction with Equations 2 and 3.

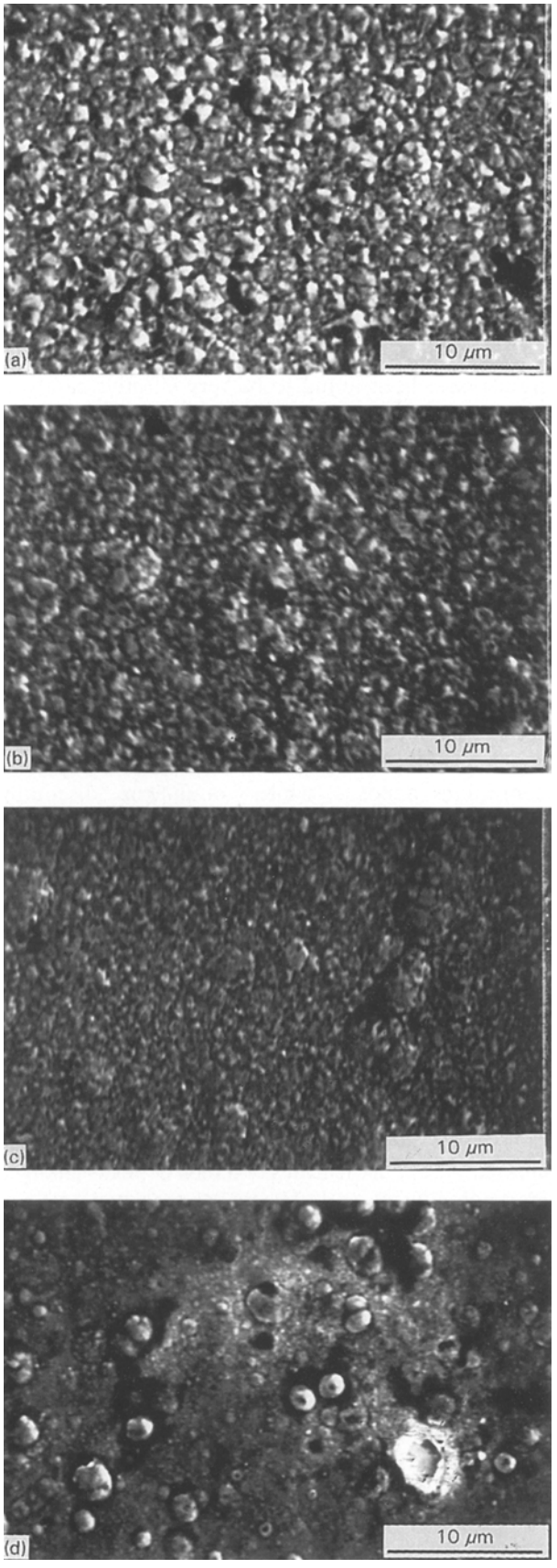

Figure 4 Surface features of LG Ni deposits (Consort I) produced potentiostatically at (a) 4.5 V, (b) 6.0 V, (c) 7.5 V, (d) 9 V with sulfamate electrolyte and Au substrate.

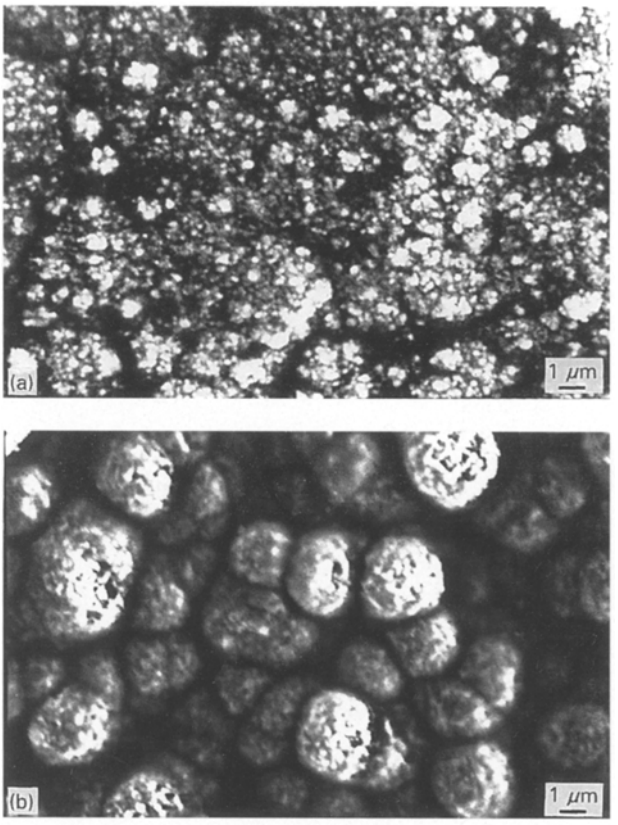

Figure 5 Surface features of (a) LG Ni deposits (Consort IV) and (b) its 1 g counterpart with sulfate electrolyte and Au substrate at 9 V.

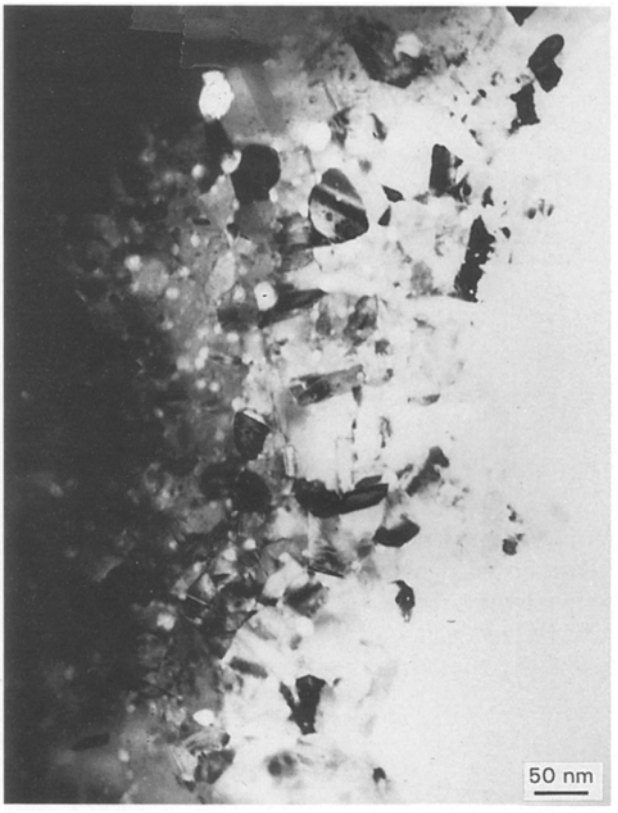

Figure 6 TEM micrograph of LG Ni deposit (Consort III) with sulfamate electrolyte and Au substrate.

TEM analysis of Ni deposits on gold showed a nonuniform distribution of crystal sizes ranging from 5–100 nm throughout the deposit thickness (Fig. 6). The crystals exhibited non-preferred orientation.

LG Ni deposits on GC peeled off the substrate completely, rendering it feasible to study sample features at the onset and finish of the deposition process. TEM micrographs showed a remarkably

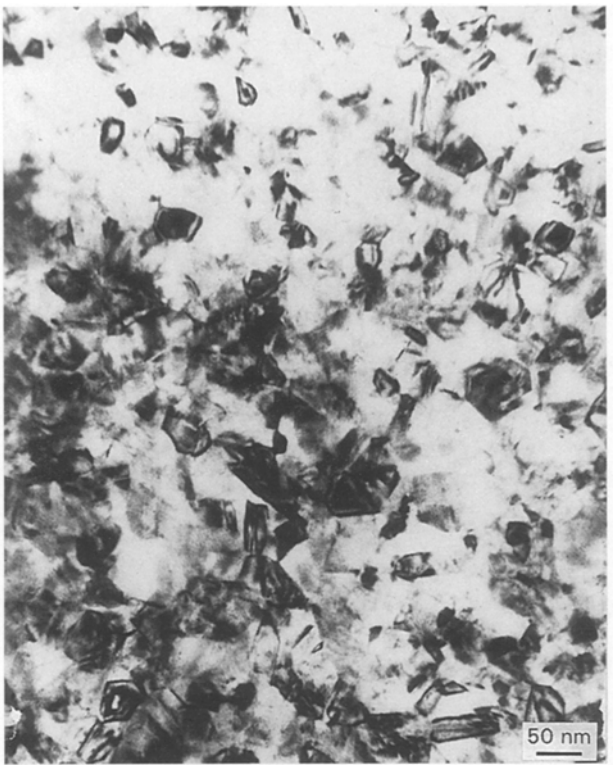

Figure 7 TEM micrograph of LG Ni deposit (Consort III) with sulfamate electrolyte and GC substrate.

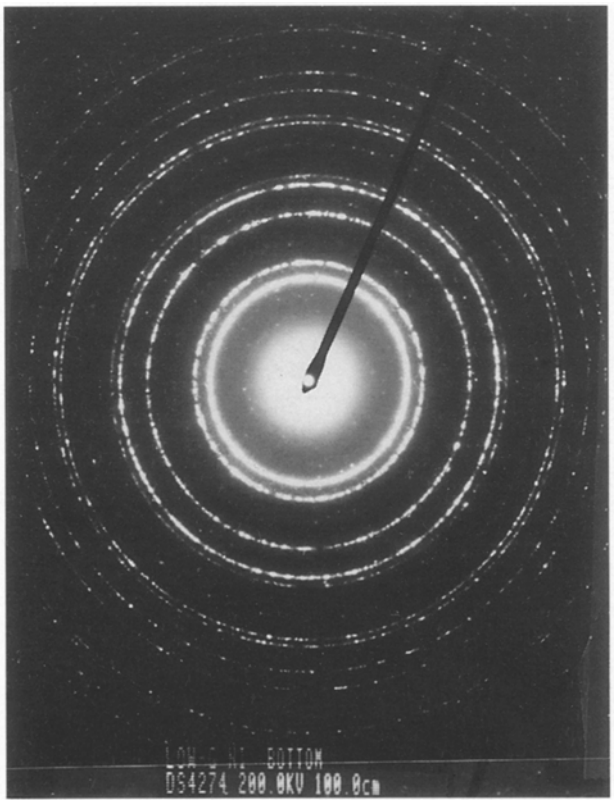

Figure 8 Diffraction pattern of sample in Fig. 7.

homogeneous grain distribution next to the substrate, with sizes of ~ 10 nm (Fig. 7). Continuous rings in the DP (Fig. 8) indicated homogeneity and finite crystallinity. Ni grains increased in size near the centre and at the surface reaching 1 μm and the twin density was considerably higher in these regions.

Epitaxial growth would not be expected in these samples owing to the high current density, the considerable misfit between Ni and Au (0.136 compared to 0.0126 between Ni and Cu) and the smooth polished substrate. Likewise epitaxial growth would not be expected on an amorphous substrate such as GC according to Choi and Weil [22]. The fine grained deposits obtained adjacent to the amorphous substrate is also in full agreement with Choi and Weil.

The lack of surface features in the high current gold substrate 9 V Ni deposit, in particular the Consort I sample, could be explained by the preference of nucleation rather than growth. The main reasons for this situation are high current density allowing adatoms to arrive in large numbers at the cathode, so they cannot diffuse to kink sites (nucleation sites) before encountering other adatoms, and heavy deformation of the substrate surface resulting from buffing or grinding [18].

3.1.3. X-ray analysis

X-ray diffraction analysis revealed the anomalities of the low-g produced deposits. XRD scans of the LG deposits produced with progressively increasing current reveal a clear trend of decreasing Ni diffraction peak intensities (Fig. 9). At 9 V the sample Ni peaks disappeared completely (at this sensitivity) indicating an amorphous or extremely fine crystalline material. One year after the flight, XRD of this sample presented small peaks corresponding to the (2 0 0) and (2 2 0) planes, implying the onset of structural changes and a tendency toward crystallization. The amorphous form of a pure metal should be thermodynamically unstable, and in the absence of stabilizing metalloids it should transform into the lower energy form with time [2].

Compared to our Consort I 9 V sample, Consort III 9 V deposits on GC exhibited sharp Ni f c c crystalline peaks and those on Au gave very small broad diffraction peaks (Fig. 10). Similar small broadened Ni peak were obtained for the potentiostatically-controlled deposition on the Consort IV experiment, except for the deposit produced at high current from a sulfate bath in a CE cell (Fig. 11). This surface was a reproduction of the 9 V Consort I sample in that no XRD was expressed by the Ni deposited surface. Extensive enhancement of the intensity scale of this sample revealed small broad Ni peaks superimposed on a noisy background (Fig. 12). 1 g counterparts produced on the bench with identical experimental parameters in a cathode over anode configuration resulted in sharply defined Ni and more intense Au substrate peaks than the corresponding LG deposits, reflecting crystalline Ni and thinner deposited films.

Peak broadening is directly related to crystal size where the smaller the crystals the broader the corresponding X-ray peaks. In order to elucidate the crystal sizes of the LG deposits, intensity profiles from the slow XRD scans were utilized in conjunction with Sherrer and Fourier analysis [23]. For the Sherrer method, Laue peak breadth rather than Sherrer peak breadth was utilized. In the former, the breadth is the

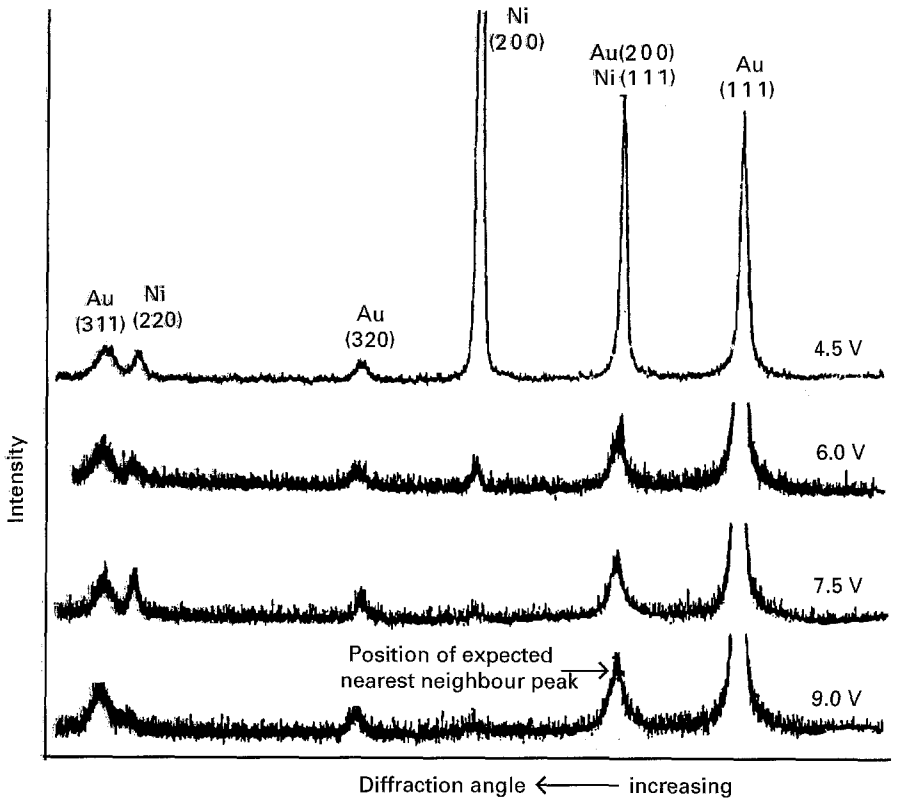

Figure 9 XRD scans of varying rate LG Ni deposits produced by different applied voltages (Consort I) with sulfamate electrolyte and Au substrates.

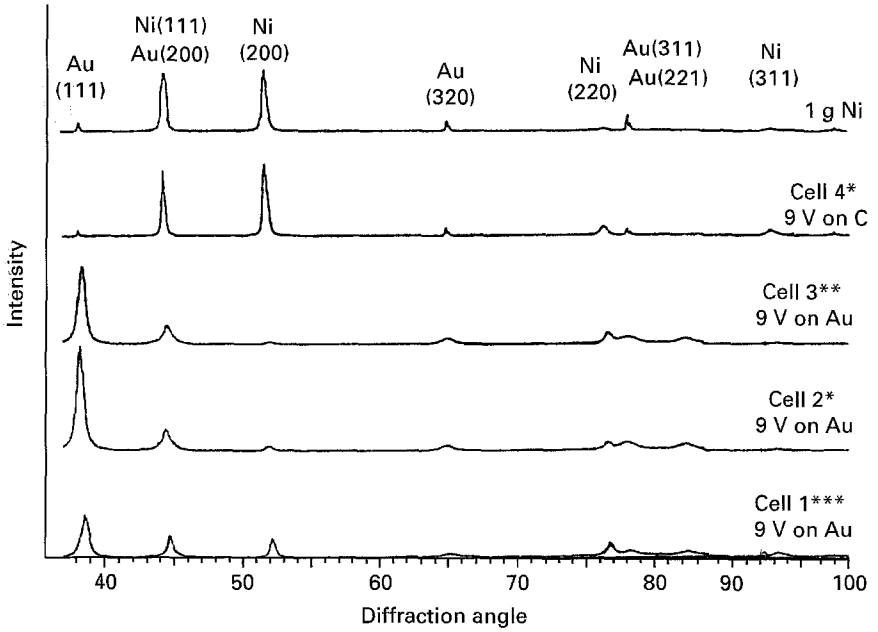

Figure 10 XRD scans of LG Ni deposits produced at 9 V (Consort III), where * designates sulfamate electrolyte, ** designates sulfate electrolyte, and *** designates sulfamate electrolyte with stirred cell.

quotient of diffraction peak area and maximum peak intensity. In the later the peak's full width at half height (fwhm) is utilized. The Laue regimen provides greater internal consistency and is thus more appropriate for application when a distribution of crystal sizes is encountered in the specimen [24]. All sizes would be contributing to the integral breadth, whereas this would not be the case in the half width values. Corrected and uncorrected values from the Sherrer method were obtained for comparison purposes. For the Fourier method, the distribution of the X-ray intensity in the samples and standard diffraction lines were expressed as Fourier series. The deconvolution of the instrumental and crystal size broadening followed

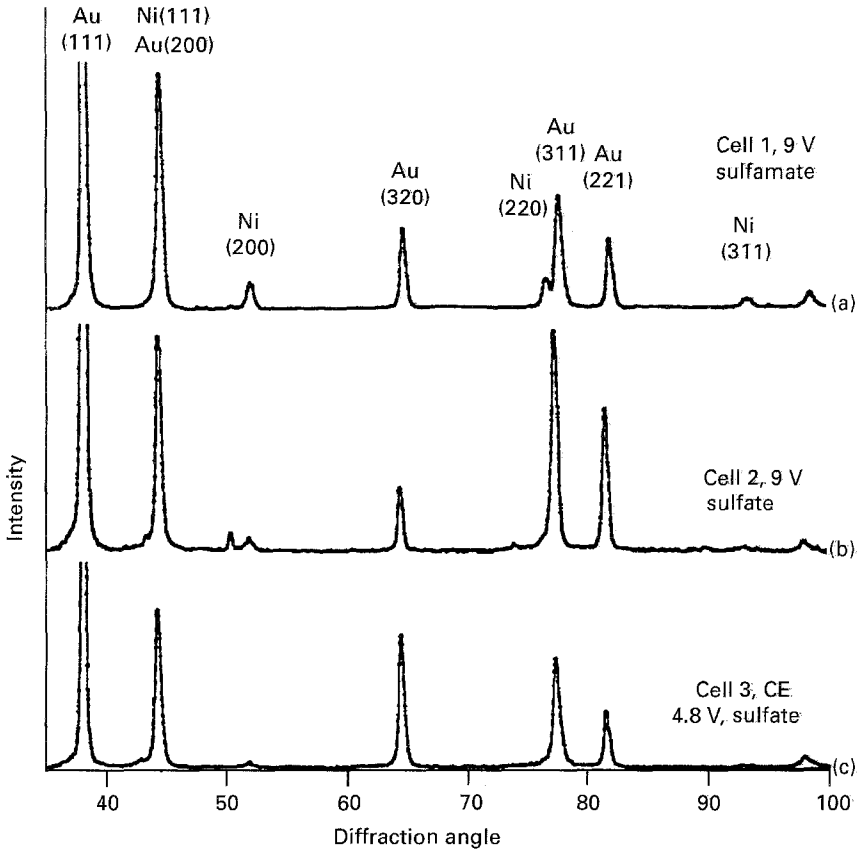

Figure 11 XRD scans of LG Ni deposits (Consort IV) on Au substrates. (a) sulfate solution at 9 V, (b) sulfamate solution at 9 V and (c) sulfate solution with close electrode at 4.8 V.

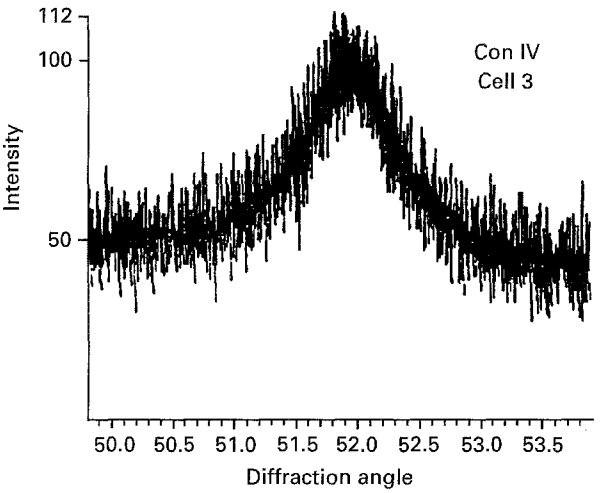

Figure 12 Enhanced XRD scan of the LG Ni (2 0 0) peak (Consort IV) of cell 3, close electrode deposit of Fig. 11.

a Fourier approach in which the X-ray intensity line $h(x)$ recorded from the specimen was expressed as

$$h(x) = \int_{-\infty}^{+\infty} f(y)\,g(x - y)\,\mathrm{d}y \qquad (4)$$

where $f(x)$ is the intensity that would be recorded in the absence of instrumental broadening, and $g(x)$ is the intensity recorded from crystallites of infinite effective size (standard), so that all the broadening is instrumental [13, 23]. Here $h(x)$ and $g(x)$ are known. Following a general approach devised by Stokes, a range of values of y from $-c/2$ to $+c/2$ outside which $g(x)$ and $h(x)$ are zero, i.e. outside this range the intensity would have fallen to its background value, is considered [25]. The deconvolution procedure yields the expression:

$$F(t) = \frac{H(t)}{c\,G(t)} \qquad (5)$$

where F, H and G are the Fourier coefficients of the functions f, h and g, respectively. The Fourier method for crystallite size determination followed a general treatment by Warren [26] and Bertaut [27] which considers a 0 0 1 powder pattern reflection from a material having orthorhombic axes. This method could be generalized to represent any hkl for any cubic crystal. The crystal considered in this method is modelled after Bertaut as columns of unit cells which are perpendicular to the reflecting plane and parallel to $\mathbf{a}_3$, where $\mathbf{a}_1$, $\mathbf{a}_2$ and $\mathbf{a}_3$ are the basis vectors of the crystal [29]. The average crystallite size was obtained from a plot of the normalized corrected Fourier coefficients versus $D(k)$, where:

$$D(k) = k\left[\frac{\lambda}{a\cos(\phi_0)}\right] \qquad (6)$$

and a is the Fourier interval (diffraction angle interval), ϕ_0 is the diffraction angle at maximum intensity and k is the Fourier harmonic.

TABLE II Average crystal sizes in nanometers of low gravity Ni deposits on Au substrates

Sample	Fourier method	Corrected Sherrer method	Uncorrected Sherrer method
Con III, 9 V stirred, sulfamate	19	22	19
Con III, 9 V sulfamate	23	26	18
Con III, 9 V sulfate	16	29	21
Con IV, 9 V sulfamate	11	14	18
Con IV, 4, 8 V CE, sulfate	10	15	22

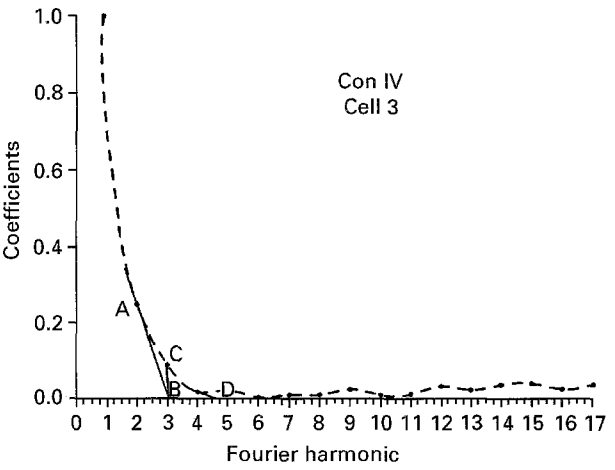

Figure 13 Crystal size distribution of Fig. 12 sample.

The x-axis intercept of the initial slope of this plot gives the crystallite size directly. Table II presents the results. Averages given in this table are semi-quantitative, intended to provide a general picture of the crystal size trends in the deposits. Inherent differences between the methods utilized, generated the differences between the average values. The Fourier method should yield values that are closest to the actual crystal sizes. The divergence of data in the first two columns is an indication of the population and crystal size distribution width in the sample. The deposit obtained from the sulfate solution in the regular cell produced the greatest difference between Fourier and corrected Sherrer methods. As will be seen later, the corrosion behaviour of this sample was also peculiar. The smallest sizes were obtained for the Consort IV CE sample. The sizes reported in Table II fall in the nanocrystalline range.

The size distribution was, in general, nonsymmetric as indicated by the differences of sizes between ABC and BCD triangles. A typical sample plot is given in Fig. 13. This observation is consistent with the TEM results. The size distribution could be attributed to the nucleation and growth processes. The high current adopted in these experiments, as well as lack of gravity, generated small crystal sizes with random distributions.

3.1.4. Hydrogen effect

A side product of the high current electrodeposition process in these experiments is gas generation by the oxidative and/or reductive reactions. H_2 is produced at the cathode and O_2 at the anode according to:

In diffusion controlled bench deposition, gases generated migrate to the top of the cell, where they accumulate. H_2 at the cathode becomes diluted with O_2, in the presence of high field some recombination might occur. In LG, gases would not migrate in the cell, hence, the highly energetic H_2 would be in contact with the freshly deposited metal and interaction between the two elements can take place with little hindrance. This could be significant especially for Ni, since it exhibits the highest H_2 capacity of any purely endothermic absorbing metal [29]. Atomic hydrogen inclusion in the Ni matrix as NiH could also lead to crystalline and morphological changes.

Based on the volume expansion provided by the rubber tubes installed in the cell sides (Fig. 1) and the efficiency charts of the electrodeposition, the pressure of H_2 in some of the cells was estimated to be 6.078 Pa. At this high pressure, H_2 is expected to be absorbed in the Ni film, and to interfere in the nucleation-growth process of the depositing metal, and mainly to impact the crystal form of the deposit.

3.1.5. Corrosion testing

Corrosion testing of the rate-study Consort I Ni deposits by method 1 (section 2.2) indicated a progressive resistance to acid etching as the rate increased. At 9 V the deposited film was not affected by the etchant, no pits were evident. Table III shows the corrosion potentials (E_c) and corrosion currents (i_0) of selected samples from subsequent flights as determined by cyclic voltammetry in sea water versus the saturated calomel electrode (SCE). A typical CV plot is shown in Fig. 14. Corrosion potentials of LG Ni surfaces from regular cells indicated higher corrosion resistance than their 1 g counterparts. In general a CE cell

cathode $2H_2O + 2e^- \rightarrow H_2(g) + 2OH^-$ $E^0 = -0.83$ V (7)

$2H^+ + 2e^- \rightarrow H_2(g)$ $E^0 = -0.00$ V (8)

$H^+ + e^- \rightarrow H\cdot,\ H\cdot + H\cdot \rightarrow H_2(g)$ (9)

anode $2H_2O \rightarrow O_2(g) + 4H^+ + 4e^-$ $E^0 = -0.25$ V (10)

TABLE III Corrosion behaviour of electrodeposited Ni films

Sample	E_0, Corrosion potential mV versus SCE		i_0, Corrosion current ($\mu A\ cm^{-2}$)	
	LG	1 G	LG	1 G
9 V, sulfamate, Con III	− 0.175	− 0.200	0.05	0.11
9 V, sulfate, Con III	− 0.150	− 0.180	0.11	0.12
9 V, sulfate, Con IV	− 0.155		0.04	
4.8 V, sulfate, Con IV, CE cell	− 0.14		0.05	

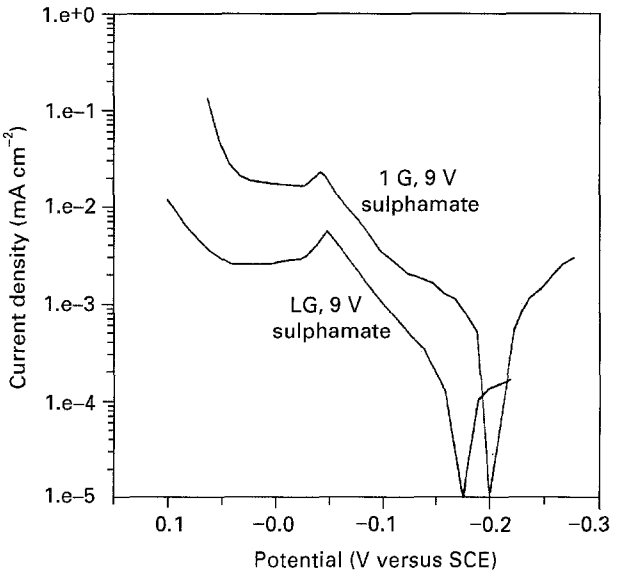

Figure 14 Cyclic voltammetry corrosion current versus potential profiles for LG and 1 g Ni deposits (Consort III).

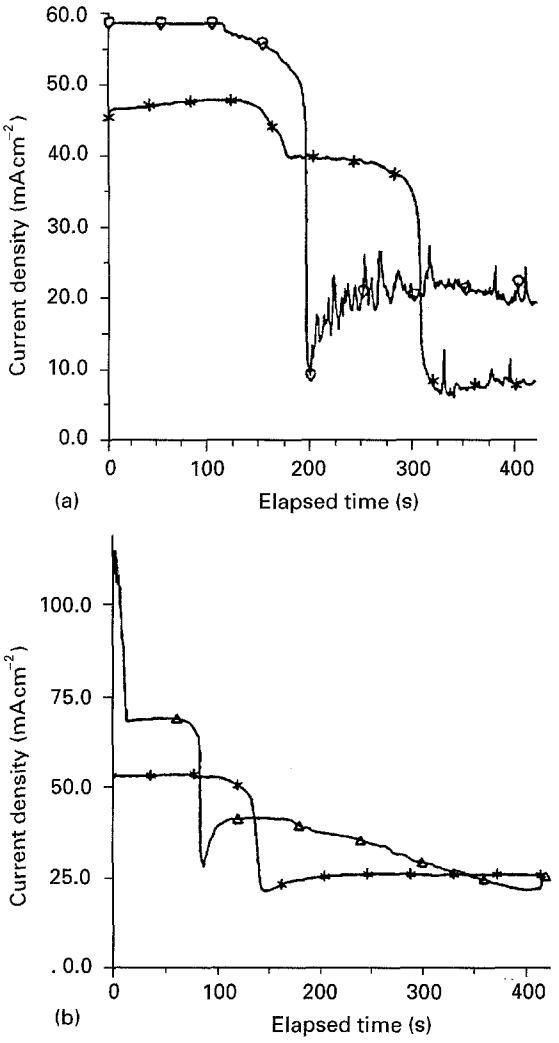

Figure 15 Current chronographs from Consort I of (a) ▽ LG, Co 5.0 V; * LG, Co 4.0 V and (b) △ 1 g, Co 5.0 V; * 1 g, Co 4.0 V.

configuration promoted higher corrosion resistance than a regular cell. The kinetics of the corrosion process, indicated by i_0, reflect a faster corrosion process for the 1 g samples (higher i_0 values) than their LG counterparts.

The corrosion resistance of the samples studied was affected by the electrolyte nature and the cell design in addition to the gravitational level. In general, metals with high numbers of active sites, abundant grain boundaries, low hydrogen atom inclusion, and slow forming nonuniform surface passive films, exhibit low corrosion resistance. Structural factors such as preferred orientation and the nature of defects in a metal also contribute to its corrosion behaviour. The amorphous character of materials, by itself, has not been proven to promote higher corrosion resistance [2]. CE cell design might promote higher hydrogen inclusion in the deposited Ni films, and consequently higher corrosion resistance.

3.2. Cobalt

Co deposition processes were potentiostatically controlled. Assuming equilibrium conditions, the low gravity, non-convective process can be described by the Cottrell equation [30] which predicts a current decrease that is inversely proportional to deposition time. Fig. 15a and b for the LG and the 1 g counterpart deposition, respectively, show remarkable similarities to each other and divergence from the behaviour predicted by the Cottrell equation. The sudden drop of current and subsequent shut-off of the deposition were attributed to an anodic passification. In this process, the Co^{2+} ions produced by the anodic oxidation reaction, recombine with the sulfate counter ions to form $CoSO_{4\,(aq)}$. When the concentration of this salt reaches saturation levels, it crystallizes and masks the anode. The higher the current the faster the drop. In LG the current levels were lower and the duration to the shut-off is longer than in 1 g. Hydrodynamics of gas generated during plating and the consequent convection in 1 g are responsible for these subtle differences. A simple shaking of the 1 g cell can produce an oscillating system [32]. The stable current throughout the process, as well as the LG–1 g similarities indicated that mass transport is not the dominating factor in this Co system. Rather, the system is kinetically controlled by the charge or crystallization overpotentials.

XRD of the Co deposits showed no structural changes in LG deposits versus 1 g. Both environments produced the expected hexagonal crystal structure.

4. Conclusions

4.1. Nickel electrodeposition

(a) In our closed cells under potentiostatic control, the high current Ni deposition under LG environment produces uniform continuous coatings. Similarly prepared 1 g counterparts are stressed and discontinuous.

(b) LG high rate deposition of Ni, reaching or surpassing 75 mA cm^{-2}, produces a form that is nanocrystalline of average crystal sizes ranging between 10 and 25 nm. The deposits could also be mixtures of amorphous and microcrystalline forms.

(c) The electrochemical factors influencing Ni deposition are different in the two environments as indicated by differences in current outputs. Mass transport plays an important role in this system. This conclusion does not rule out crystallization and/or charge transfer as important factors as well.

(d) Galvanostatic control of the high current electrodeposition process in LG does not produce satisfactory plating films in our cells. Instead, partial noncontinuous deposits are obtained.

(e) Gas generated during the deposition process exhibits different hydrodynamics in LG than in 1 g. The hydrogen evolved at the cathode could have seriously impacted the crystallinity of the deposited Ni.

4.2. Cobalt electrodeposition

(a) Electrodeposition in low gravity does not induce structural changes in cobalt deposits at the deposition currents utilized here. A different solution enabling higher currents might induce change.

(b) The electrochemical factors influencing the Co systems are not affected by the lack of the gravitational force as indicated by the similarities in current outputs in the two environments. This implies that kinetic control rather than mass transport is the controlling factor in this system.

Acknowledgement

The financial support of McDonnell Douglas Corporation and NASA through the Center for Materials Development in Space at the University of Alabama in Huntsville is gratefully acknowledged. The authors thank H. Dwain Coble, McDonnell Douglas engineers for their technical assistance and Dr. D. Schwartz for the TEM data.

References

1. NATIONAL RESEARCH COUNCIL, "Materials Science and Engineering for the 1990's" (National Academy Press, Washington, DC, 1989).
2. F. E. LUBORSKY (Ed.), "Amorphous Metallic Alloys" (Butterworth & Co Ltd., London, 1983) 1.
3. R. DAGANI, *Chem. Eng. News* **23** (1992) 18.
4. J. MASIL, *Met. Finish.* **78** (1990) 480.
5. G. E. RENDON, (Ed.), "Materials Processing in the Reduced Gravity Environment of Space" (Elsevier Science Publishing Company, Inc., London, 1982).
6. G. A. HAZELRIGG and J. M. RYNOLDS (Eds), "Opportunities for Academic Research in a Low Gravity Environment", Vol. 108 (Progress in Astronautics and Aeronautics, 1986).
7. F. C. WESSLING, C. A. LUNQUIST, G. W. MAYBEE, *Acta Astronaut.* **21** (1990) 647.
8. C. RILEY, H. ABI-AKAR, B. BENSON and G. MAYBEE, *J. Spacecr. Rockets* **27** (1990) 4.
9. J. EHRHARDT, *Galvanotecnik*, **72** (1981) 13
10. *Idem*, Dispersion Electrolysis Under Zero Gravity Under SPACELAB Rocket Program TEXUS IV. Battele Institute, BMFT Reference No. QV 219-AK-AN/A-ALN 710 (April 1982).
11. *Idem*, TEXUS VII, BMFT Reference No. 01 QV 219-AK-AM/A-SLN 7910-5 (November 1983).
12. *Idem*, TEXUS IX, BMFT Reference No. 01 QV 014-AK/SN (November 1984).
13. H. ABI-AKAR, Dissertation, "Electrodeposition in Low Gravity", The University of Alabama in Huntsville, AL, USA (1992).
14. J. K. DENNIS and T. E. SUCH, "Nickel and Chromium Plating" (Halsted Press Division John Wiley and Sons, Inc. 1972) 48.
15. H. J. S. SAND, *Phil. Mag.* **1** (1900) 45
16. *Idem*, *Z. Physik. Chem.* **35** (1900) 614.
17. H. FEIGENBAUM and R. WEIL, *J. Electrochem. Soc.* **126** (1979) 2085.
18. W. KIM and R. WEIL, *Surf. Coat. Tech.* **31** (1987) 143.
19. G. C. YE and D. N. LEE, *Plat. Surf. Finish.* **68** (1981) 60.
20. G. C. YE and D. N. LEE, *ibid.* **68** (1981) 46.
21. R. WEIL and W. N. WU, *Plat.* **60** (1973) 622.
22. H. J. CHOI and R. WEIL, *Plat. Surf. Finish.* **68** (1981) 110.
23. A. TAYLOR, "X-Ray Metallography" (John Wiley & Sons, Inc. New York, 1961).
24. C. G. SHULL, *Phys. Rev.* **70** (1946).
25. A. R. STOKES, *Proc. Phys. Soc. (London)* **61** (1948) 382.
26. B. E. WARREN, *Prog. Met. Phys.* **8** (1959) 147.
27. E. F. BERTAUT, *Comput. Rend.* **228** (1949) 492.
28. B. E. WARREN, *Acta. Crystallogr. Camb.* **8** (1955) 483.
29. W. M. MUELLER, J. P. BLACKLEDGE and G. G. LIBOWITZ, "Metal Hydrides" (Academic Press, New York and London, 1968).
30. F. G. COTTRELL, *Z. Physik. Chem.* **42** (1903) 385.
31. C. RILEY, H. D. COBLE, B. LOO, B. BENSON, H. ABI-AKAR and G. MAYBEE, *Polym. Preprints* **28** (1987) 470.

Received 31 August 1994
and accepted 19 September 1995